Journal of Alloys and Compounds 509 (2011) 4574–4582

Contents lists available at ScienceDirect

Journal of Alloys and Compounds

journal homepage: www.elsevier.com/locate/jallcom

Microstructural evolution and tensile properties of Sn–5Sb solder alloy containing small amount of Ag and Cu

A.A. El-Daly[a,*], A. Fawzy[b], A.Z. Mohamad[a], A.M. El-Taher[a]

[a] Physics Department, Faculty of Science, Zagazig Univ., Zagazig, Egypt
[b] Physics Department, Faculty of Education, Ain Shams Univ., Cairo, Egypt

ARTICLE INFO

Article history:
Received 8 November 2010
Received in revised form 16 January 2011
Accepted 18 January 2011
Available online 22 January 2011

PACS:
62.20.Fe
61.82.Bg
61.66.Dk

Keywords:
Lead-free solder
Sn–Sb alloys
Microstructure
Mechanical properties

ABSTRACT

The near peritectic Sn–5Sb Pb-free solder alloy has received considerable attention for high temperature electronic applications, especially on step soldering technology, flip-chip connection. In the present study, a separate addition of the same amount of Ag and Cu are added with the near-peritectic Sn–5Sb solder alloy to investigate the effect of a third element addition on the microstructural, thermal and mechanical properties of the newly developed ternary solder alloys. The results indicate that the melting point of Sn–5Sb solder is enhanced by Ag and Cu additions. Besides, the Ag and Cu content refine the microstructure and form new intermetallic compounds (IMCs) with the near-peritectic Sn–5Sb solder alloy. The tensile tests revealed that all alloys exhibit higher mechanical strength with increasing strain rate and/or decreasing testing temperature, suggesting that the tensile behavior of the three alloys is strain rate and temperature dependence. The yield and ultimate tensile strength are higher for Sn–5Sb–0.7Cu alloy compared with Sn–5Sb and Sn–5Sb–0.7Ag alloys. Good mechanical performance of Sn–5Sb–0.7Cu solder is often correlated to a fine β-Sn grain size and more dispersed Cu-Sn IMC particles, which makes the solder exhibit high strength and yield stress.

1. Introduction

Owing to the realization of the harmful influence of lead and lead containing alloys on the environment and human health, many Pb-free solder-alloys have been developed to replace Sn–Pb solders in electronic applications [1]. The near peritectic Sn–5Sb Pb-free solder alloy has received considerable attention for high temperature electronic applications, especially on step soldering technology, flip-chip connection [2–4], solder ball connections and bonding a semiconductor device onto a substrate. It also has proposed as cathode materials for use in lithium ion batteries [5,6]. Although demand for higher I/O counts on chips requires finer pitches to improve performance, cost effectiveness and higher yield, such increases in I/O density lower the conventional pitches to very fine sizes (20 μm). Since one role of the solder alloys is to serve as a structural material to connect the components, one of the major concerns in the development of electronic packaging is the reliability of the solder joints [7]. A viable approach to improve the performance of a solder joint in terms of low melting point, higher strength, better microstructure properties, and high creep resistance is to add appropriate second phase particles, of a ceramic, metallic or intermetallic, to a solder matrix [1,8,9].

Recently, lead-free Sn–Sb solders have been identified as potential materials with higher microstructure stability and better mechanical properties as compared to conventional Sn–Pb solders [10–12]. The addition of hard obstacles to dislocation motion can have profound effects on the tensile strength and creep resistance of a metal. Precipitation and dispersion strengthening have received significant attention in the fields of high-temperature structural materials due to markedly better creep resistance. El-Daly et al. [8] studied the influence of Ag and Au additions on the physical properties of Sn–Sb solder alloy. Mechanical and thermal property measurements indicated significant increase in creep resistance, rupture time with the alloying of Ag and Au elements. However, addition of Au can improve the melting temperature and increase fusion heat of Sn–5Sb alloy. Chen et al. [13] studied the interfacial reactions in the Sn–Sb/Ag and Sn–Sb/Cu couples and reported that all the reaction products of IMCs could grow linearly with the square root of reaction time, which suggest that the interfacial reactions are diffusion controlled. For the reliability of Sn–5Sb Pb-free solder alloy, Alam et al. [9] reported also that additions of Ag and Au into the Sn–5Sb alloy can enhance the solder properties, such as the ultimate tensile strength (UTS), ductility, and fusion heat. This is because the formation of intermetallic compounds (IMCs) $AuSn_4$ and Ag_3Sn can enhance the microstructure stability

* Corresponding author.
E-mail address: dreldaly99@yahoo.com (A.A. El-Daly).

0925-8388/$ – see front matter © 2011 Elsevier B.V. All rights reserved.
doi:10.1016/j.jallcom.2011.01.109

and retains the formation of SbSn precipitates in the solidification microstructure, thus significantly improves their strength and ductility. For all alloys, it was found that the UTS and yield stress YS increase with increasing strain rate and decrease with increasing temperature in tensile tests, but changes in ductility are generally small with inconsistent trends. However, the result of a literature search revealed that little studies have been reported on lead-free Sn–5Sb solder joints containing small amount of Ag and Cu. In this work, the incorporation of the same amount of Ag and Cu to Sn–5Sb Pb-free solder alloy was studied. Microstructural and mechanical data of the ternary solder alloys were measured and compared with the Sn–5Sb solder alloy. The effect of strain rate and temperature during mechanical testing has been studied. Correlations between the evolution of the microstructure and mechanical testing properties are proposed. The results are wished useful in the further development of new solder alloys for different electronic packaging applications.

2. Experimental procedures

In the present work, characterizations of the microstructure and tensile behavior were conducted on three lead-free solder alloys with the compositions (wt.%) of Sn–5Sb, Sn–5Sb–0.7Ag and Sn–5Sb–0.7Cu. The lead-free solders were prepared from Sn, Sb, Ag and Cu (Purity 99.97%) as raw materials. The process of melting was carried out in a vacuum arc furnace under a high purity argon atmosphere to produce rod-like specimen with a diameter of approximately 10 mm. The melt was held at 500 °C for 2 h to complete the dissolution of Sn, Sb, Ag and Cu and then poured in a steel mold to prepare the chill cast ingot. A cooling rate of 6–8 °C/s was achieved, so as to create the fine microstructure typically found in small solder joints in microelectronic packages. Table 1 lists the actual chemical compositions of the experimental alloys used in this investigation. A solution of 2% HCl, 3% HNO_3 and 95% (vol.%) ethyl alcohol was prepared and used to etch the samples. The evolution of microstructure with the Ag and Cu contents in the Sn–5Sb solder alloy was studied using optical and scanning electron microscopy (SEM) with an energy dispersive X-ray spectrometer (EDS) after etching. Phase identification of the alloy samples was carried out by X-ray diffractometry (XRD) at 40 kV and 20 mA using Cu Kα radiation with diffraction angle (2θ) from 25° to 85° and a constant scanning speed of 1°/min. Differential scanning calorimetry (DSC) (shimadzu DSC-50) was carried out to understand the melting process of the three solder alloys. Heating the specimens in DSC was carried out at 5 °C/min of heating rate in Ar flow. The solder ingots were then mechanically machined into a wire samples with a gauge length marked 3×10^{-2} m for each sample and 2.0 mm in diameter. To obtain samples containing a fully precipitated phases, the samples were annealed at 130 °C for 15 min, then left to cool slowly to room temperature. Tensile tests were carried out with a tensile testing machine (Instron 3360 Universal Testing Machine). The tests were conducted at room temperature using strain rates ranging from 10^{-3} to 10^{-2} s^{-1} to determine the effect of Ag and Cu contents on the mechanical properties of mixed alloy as well as to determine the effect of strain rate on strength. Also, the tests were conducted at different temperatures ranging from 25 to 120 °C with a constant strain rate of 1.2×10^{-2} s^{-1} to obtain data on the stress–strain curves, which contain information of elongation at fracture and UTS. Each datum represents an average of three measurements. The environment chamber temperature could be monitored by using a thermocouple contacting with specimen.

3. Results and discussion

3.1. Microstructure change with addition of Ag and Cu

X-ray diffraction analysis was performed to determine the phase composition of the IMCs particles in the three as-cast Sn–5Sb, Sn–5Sb–0.7Ag and Sn–5Sb–0.7Cu alloys. As can be seen in Fig. 1, all the three as-cast alloys are mainly composed of peaks indexed to a tetragonal cell of Sn with $a = 0.584$ and $c = 0.319$ nm and precipitated SbSn phase. The Ag_3Sn phase was found in the XRD pattern of Sn–5Sb–0.7Ag alloy, indicating the successful alloying of Sn and Ag after the melting process. At the same time, the Cu_6Sn_5 and Cu_3Sn phases were formed, which were due to the alloying of Sn and Cu in the Sn–5Sb–0.7Cu alloy. Moreover, the relative intensity of β-Sn was found to be slightly decreased with the addition of Cu, due to the formation of Cu_6Sn_5 and Cu_3Sn phases.

The microstructural evolution of the Sn–5Sb-based alloys plays a vital role in determining the mechanical properties of these alloys.

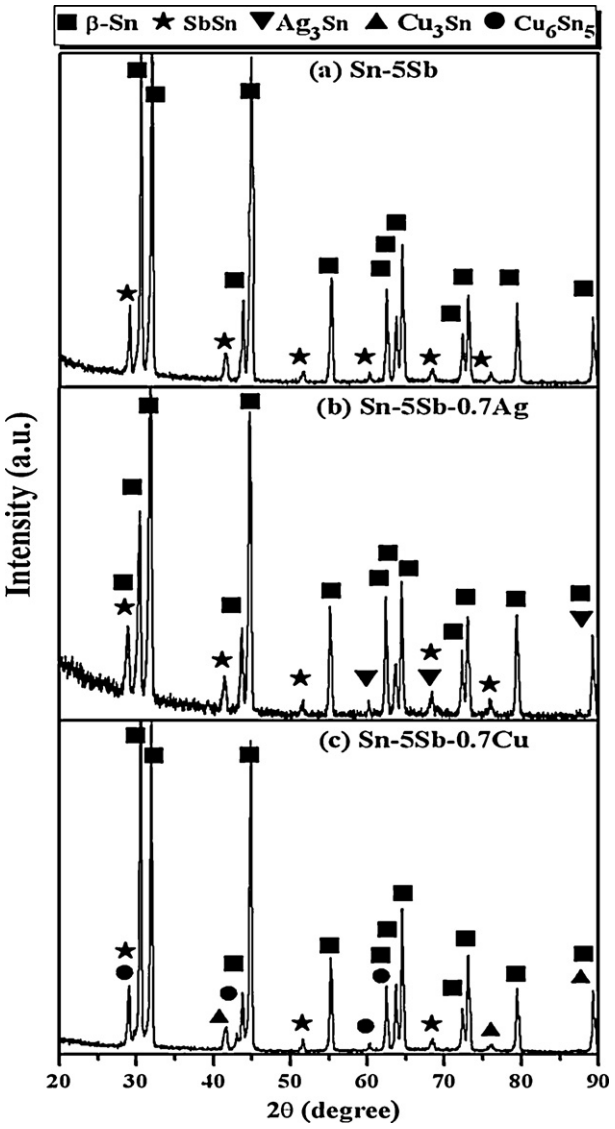

Fig. 1. XRD patterns of (a) Sn–5Sb, (b) Sn–5Sb–0.7Ag and (c) Sn–5Sb–0.7Cu solder alloys.

Fig. 2 illustrates the ability of alloying elements to refine the grain size of Sn–5Sb, indicating that Cu was significantly stronger than Ag. In Fig. 2(a), it is generally observed that the Sn–5Sb Pb-free alloy exhibits typical near-peritetic Sn–5Sb microstructure [14,21] composed of light gray areas of equiaxed β-Sn grains and dark network-like eutectic regions of SbSn and Sn phases precipitated at the grain and grain boundaries. As the sample was a hypoeutectic composition, the volume ratio of the β-Sn phase was very high and its grain size was relatively large (40 μm). With the addition of Ag into the Sn–5Sb Pb-free solder alloy, the morphology of the β-Sn phase in the Sn–5Sb alloy gradually changes from equiaxed β-Sn grains to a relatively fine dendritic β-Sn shape with the average size less than 30 μm (Fig. 2(b)). The resultant solder alloy contains a segregated phase that appears dark or black in the interdendritic regions. It has been reported that primary Ag_3Sn IMCs might act as heterogeneous nucleation sites for Sn dendrites upon solidification [20]. According to the XRD results shown in Fig. 1(b), the ternary eutectic regions were β-Sn phase, SbSn and Ag_3Sn intermetallic compounds (IMCs). Compared with the equiaxed and fine dendritic shapes of β-Sn phase observed in Sn–5Sb and Sn–5Sb–0.7Ag alloys, respectively, the same content of Cu in the Sn–5Sb solder was found to alter the microstructure of the newly developed alloy

Table 1
Actual compositions of the experimental alloys, wt.%.

Experimental alloys	Ag	Cu	Fe	Pb	Bi	Sb	As	Sn
Sn–5Sb	0.004	0.008	0.006	0.012	0.007	5.016	0.006	Bal.
Sn–5Sb–0.7Ag	0.715	0.009	0.007	0.014	0.009	5.013	0.008	Bal.
Sn–5Sb–0.7Cu	0.046	0.699	0.009	0.013	0.010	5.011	0.009	Bal.

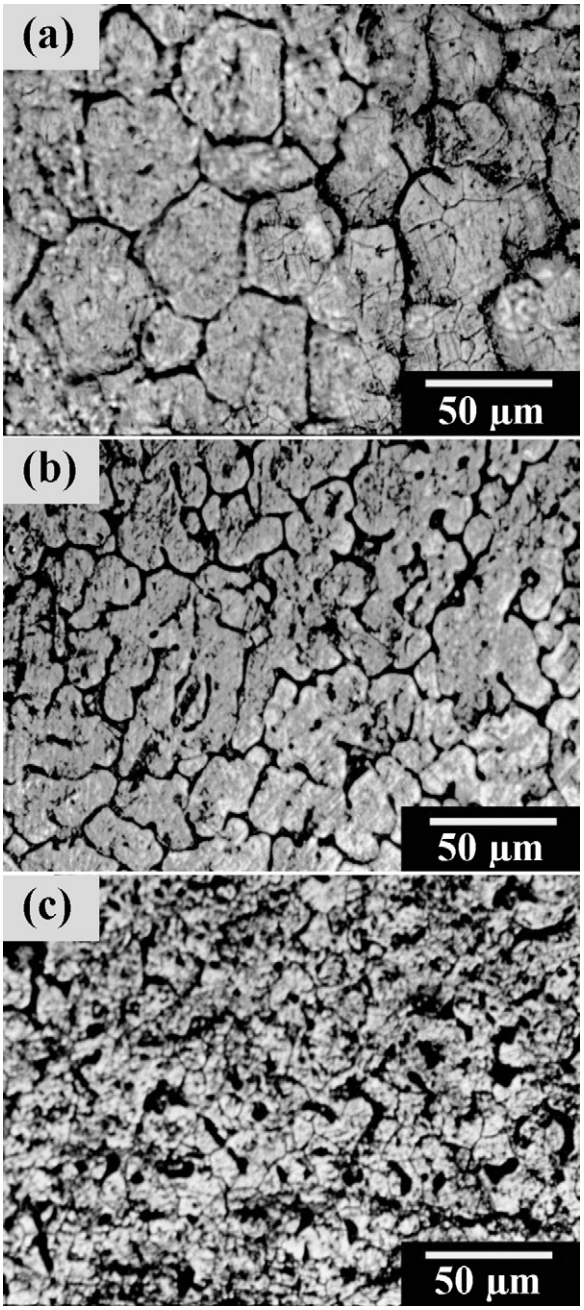

Fig. 2. OM microstructures of (a) Sn–5Sb, (b) Sn–5Sb–0.7Ag and (c) Sn–5Sb–0.7Cu solder alloys, respectively.

as shown in Fig. 2(c). Results revealed significant improvement in the refinement of β-Sn grains due to the formation of Cu_6Sn_5 and Cu_3Sn phases. The fine equiaxed β-Sn grains were found to be uniformly distributed with the average size less than 15 μm. Most of the Cu_6Sn_5 and Cu_3Sn IMCs in the Sn–5Sb–0.7Cu solder alloy were in the irregular and blocky shape imbedded in β-Sn matrix, which will lead to high strength because of precipitate strengthening mechanism [23].

To further assess the microstructural evolution of the present alloys, SEM and corresponding EDS analysis of pure Sn–5Sb-based solder alloy and two ternary alloys are shown in Fig. 3. In Fig. 3(a), the microstructure of near-peritetic Sn–5Sb alloy comprising the light gray area of extended β-Sn matrix and some irregular and heterogeneous shape of SbSn IMC particles. According to the Sn–Sb equilibrium binary phase diagram [15], although the Sn_3Sb_2 was the first form at the beginning of IMC formation, it decomposed into SbSn solid solution (β phase) and β-Sn solution at 242 °C. Similar results were also observed in Sn–10Sb–5Cu solder alloy obtained by Zeng et al. [16]. The SbSn phases were identified by XRD results and confirmed with the EDS analysis presented in Table 2. It is interesting to note that the atomic ratio of Sn to Sb at position A is about 1:1, and that of position B is approximately 25:1. This assessment implies that the dark gray phase at position A was the SbSn IMC, while the small amount of Sb (2.94%) in region B was dissolved in the β-Sn rich phase, which has the ability to increase the strengthening effect of Sn-rich phase by solid solution hardening mechanism.

However, the addition of Ag or Cu can refined the β-Sn rich phase to some extent and developed some new IMCs in the solder matrix. Fig. 3(b) shows the SEM image of Sn–5Sb–0.7Ag alloy. A small addition of Ag into the Sn–5Sb alloy produced many small spheroidal particles with a diameter less than ~1.0 μm within the like-eutectic regions and they were determined to be Ag_3Sn IMC phase by compositional analysis (Position C). Besides, the addition of Ag in the solder based alloy led to slight decrease in the overall size of the SbSn IMC precipitates (Position D). With the addition of the same amount of Cu into the Sn–5Sb alloy, the morphology of the SbSn IMCs and β-Sn rich phase was also reduced. The reason may be that the Cu addition promotes a high nucleation density of the second phase in the Sn–5Sb during solidification. EDS analysis of the needle-like phases revealed that they are composed of Cu and Sn with the Cu percentage of about 41.51 at.% (Position E). This observation implies that the needle-like phases are the Cu_6Sn_5 IMCs, while the Cu_3Sn IMC is not detected. Also, the fine particles dispersed in the β-Sn phase were determined to be SbSn IMC phase using compositional analysis (Position F).

3.2. Melting temperature (T_m) of solders

Fig. 4 illustrates the DSC curves of the three solder alloys upon heating. The results are summarized in Table 3. It is found that additions of small amount of Ag or Cu metals to Sn–5Sb alloy provided a marked improvement in melting characterization properties. The T_m of Sn–5Sb at the endothermic peak is 239. 2 °C. The only endothermal peak for Sn–5Sb samples was separated into two regions of heat extraction that are indicative of melting temperature for Ag-containing samples (Sn–5Sb–0.7Ag). The first peak at low temperatures is the eutectic temperature of the Ag_3Sn–Sn binary system [15], and the second peak at high temperatures corresponded to the melting temperature of the primary β-Sn phase and the liquidus line of the newly developed ternary solder alloy. The addition of 0.7 Cu further depressed the T_m of Sn–5Sb alloy to 233.8 °C. However, from the DSC curves, it is clear that Cu is more effective than Ag in dropping the melting temperature of Sn–5Sb-based lead-free solders. Moreover, the addition of Cu expands slightly the temperature interval of the pasty range

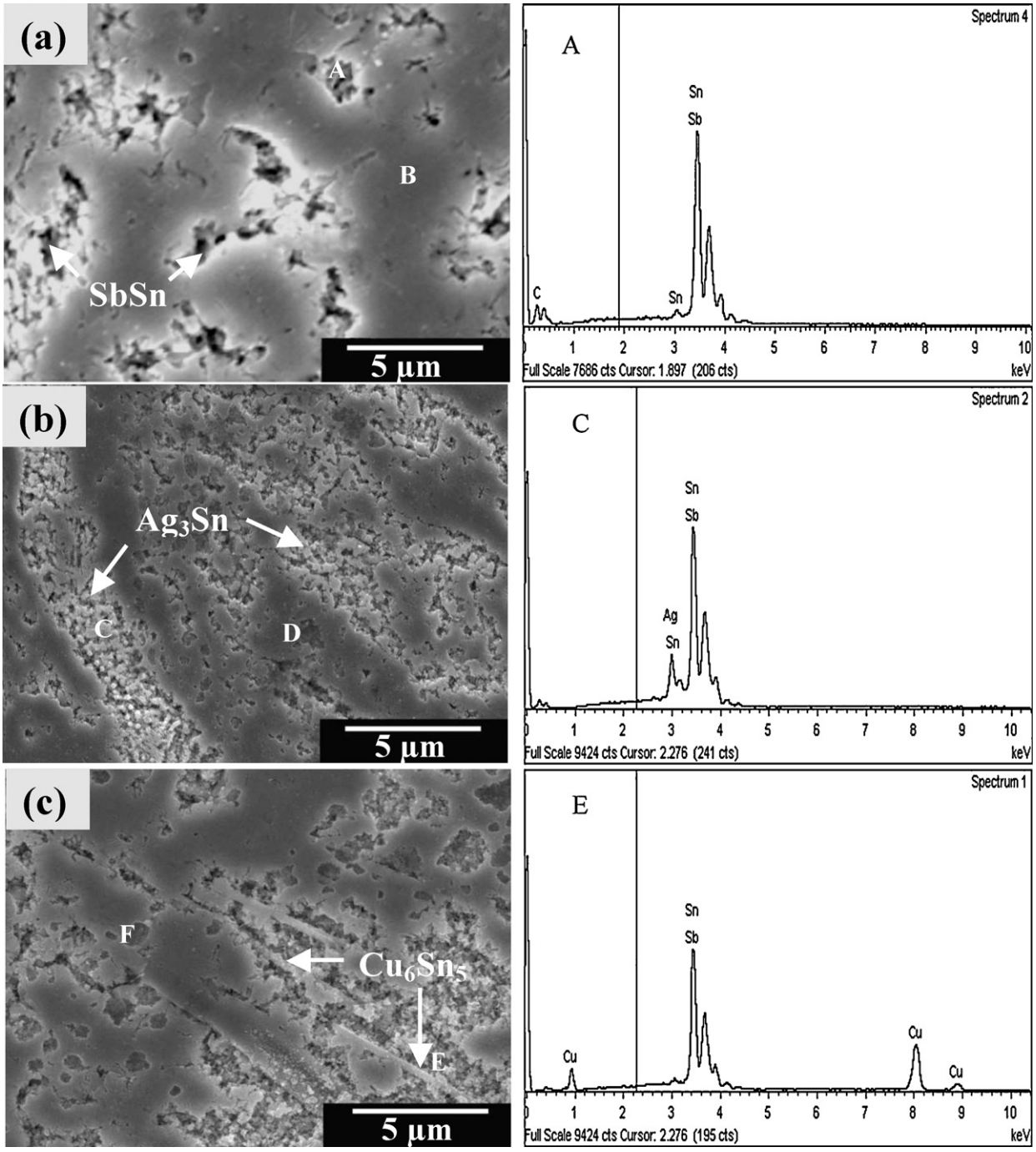

Fig. 3. SEM microstructures of (a) Sn–5Sb, (b) Sn–5Sb–0.7Ag and (c) Sn–5Sb–0.7Cu solder alloys, and the corresponding EDS analysis of some locations.

Table 2
Chemical compositions of phases formed in Sn–5Sb, Sn–5Sb–0.7Ag and Sn–5Sb–0.7Cu solder alloys.

Alloy	Position	Phase	Compositions (at. %)			
			Sn	Sb	Ag	Cu
Sn–5Sb A	A	SnSb	51.08	48.92		
	B	β-Sn	97.06	2.94		
Sn–5Sb–0.7Ag C	C	Ag_3Sn	51.06	1.89	20.22	
	D	SnSb	51.06	48.94		
Sn–5Sb–0.7Cu E	E	Cu_6Sn_5	56.34	2.15		41.51
	F	SbSn	51.15	48.85		

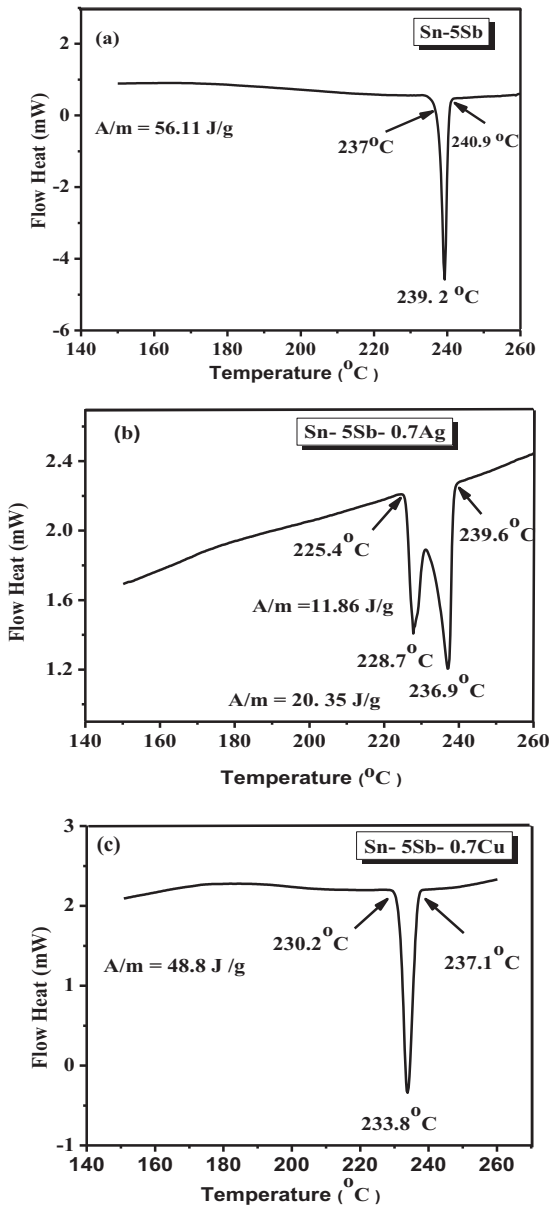

Fig. 4. DSC heating curves for solder alloys with the composition (a) Sn–5Sb, (b) Sn–5Sb–0.7Ag and (c) Sn–5Sb–0.7Cu.

(T_{end}–T_{onset}) from 3.9 to 6.9 °C, whereas the addition of Ag increases it to 14.2 °C. This large pasty range increases the tendency towards porosity and hot tearing due to the effect of alloy shrinkage and differential thermal contraction during solidification. Thus, a small addition of Cu to Sn–5Sb alloy is expected to prevent the formation of solidification defects caused by large pasty range.

3.3. Tensile properties

The effect of Ag and Cu additions on the mechanical properties of Sn–5Sb solder can be seen from stress–strain curves shown in Fig. 5. Table 4 and Fig. 6 list the average values of ultimate tensile stress (UTS), yield stress (YS) and elongations at T = 90 °C and strain rate of 1.2×10^{-2} s^{-1}. The UTS values of Sn–5Sb, Sn–5Sb-0.7Ag, and Sn–5Sb–0.7Cu were 32.4, 34.3 and 40.0 MPa, respectively. The elongation at failure of Sn–5Sb, Sn–5Sb–0.7Ag, and Sn–5Sb–0.7Cu were 60%, 62.5%, and 69.0%, respectively. The Sn–5Sb–0.7Cu alloy had both the highest UTS and elongation, while Sn–5Sb alloy had the lowest one. One possible reason for increasing the UTS of

Table 3
Comparison of solidus temperature (T_{onset}), liquidus temperature (T_{end}), pasty range (T_{onset}–T_{end}) and melting temperature (Peak) for various solder alloys during heating.

Alloy	T_{onset} (°C)	T_{onset} (°C)	Pasty range (T_{onset}–T_{end})	Melting tempertaure	
				(Peak 1)	Peak (2)
Sn–5Sb	237.0	240.9	3.9	239.2	
Sn–5Sb–0.7Ag	225.4	239.6	14.2	228.7	236.9
Sn–5Sb–0.7Cu	230.2	237.1	6.9	233.8	

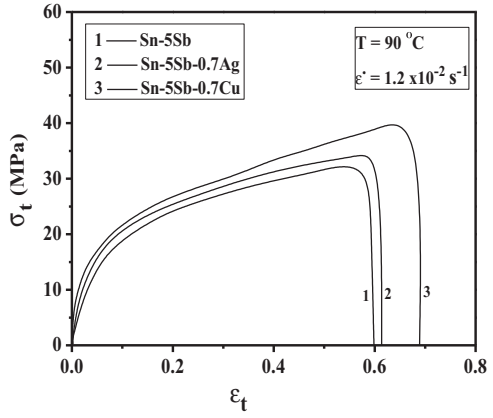

Fig. 5. Comparative tensile stress–strain curves obtained at T = 90 °C and strain rate of 1.2×10^{-2} s^{-1} for Sn–5Sb, Sn–5Sb–0.7Ag and Sn–5Sb–0.7Cu solder alloys.

Sn–5Sb–0.7Cu alloy is the hardest and softest nature of Sn–Cu and SbSn IMCs in this alloy, respectively. It is also interesting to note that the enhanced ductility of Sn–5Sb–0.7Cu alloy is achieved without sacrificing the mechanical strength. However, after the stress levels climb up to YS of the solder alloys, the strain hardening, instead of strain softening, has occurred in all the as-solidified solder alloys, which may enhance the UTS and YS in these alloys [19]. Since the deformation resistance of solder alloy was defined crucial mechanical property, a good deformation resistance implies large plastic region [8]. Compared with the Sn–5Sb alloy and Sn–5Sb–0.7Ag alloy solders, which have a slight deformation resistance, an excellent deformation resistance and long plastic region of Sn–5Sb–0.7Cu alloy would insure this solder to become one of candidate for substituting the Sn–5Sb solder in microelectronic packaging and interconnecting. The addition of 0.7% Cu was sufficient to induce a significant change in the mechanical properties. This indicates that the resistance to necking has been improved due to the high interface formed between SbSn and Cu_6Sn_5 IMCs with the β-Sn matrix, which in turn enhanced both UTS and elongation [8,19]. These results also are consistent with the findings of other researchers working on Sn-based solder alloys [10,18,19,26]. On contrast, the Ag_3Sn IMCs particles formed in the Sn–5Sb–0.7Ag alloy can slightly enhance the UTS of this solder due to small elastic modulus of these IMCs inside the solder matrix. These results are consistent with the previous finding [22] that the Cu_6Sn_5 often exhibits a larger elastic modulus than Ag_3Sn IMCs when alloying 0.7Cu and 1.5 Ag to Sn–9Zn solder, respectively.

Table 4
Tensile properties of the solders Sn–5Sb, Sn–5Sb–0.7Ag and Sn–5Sb–0.7Cu solder alloys at T = 90 °C and $\varepsilon' = 1.2 \times 10^{-2}$ s^{-1}.

Alloy	YS (MPa)	YS (MPa)	Elongation (%)
Sn–5Sb	7.3	7.3	60.0
Sn–5Sb–0.7Ag	9.9	9.9	62.5
Sn–5Sb–0.7Cu	12.2	12.2	69.0

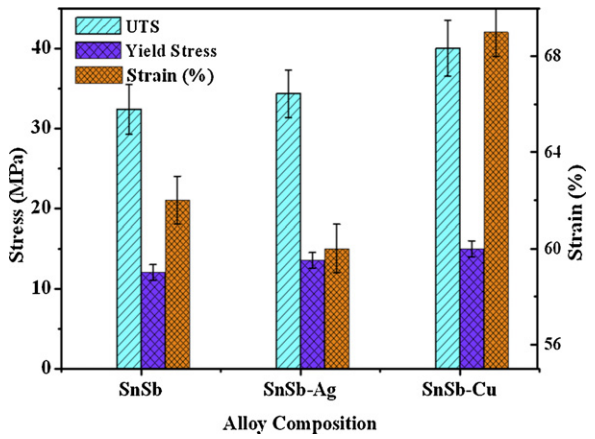

Fig. 6. Mechanical properties of Sn–5Sb, Sn–5Sb–0.7Ag and Sn–5Sb–0.7Cu solder alloys.

3.4. Effect of strain rate on the mechanical properties

Fig. 7 shows the effect of strain rate on UTS, YS and elongations of the three solder alloys at 90 °C. The entire alloys demonstrated

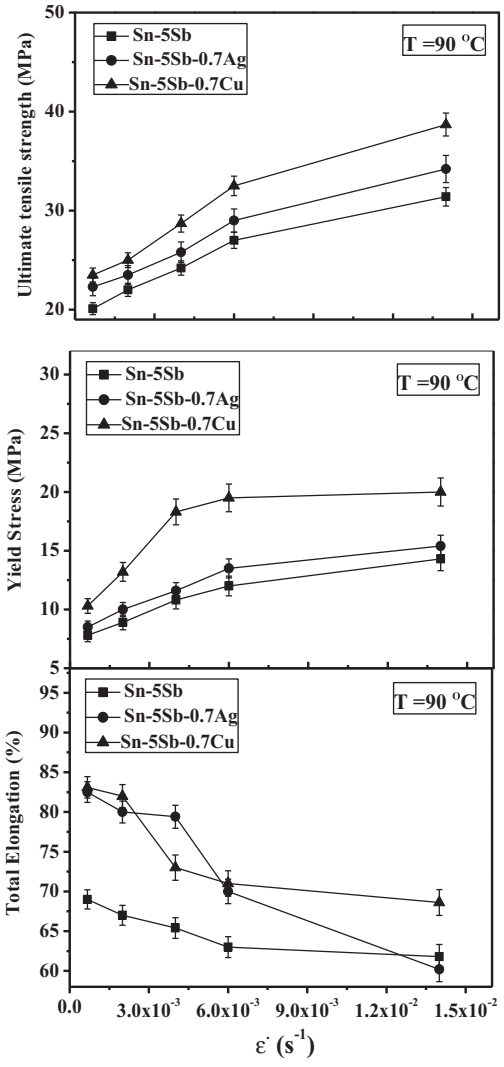

Fig. 7. Effect of strain rate on: ultimate tensile strength (UTS), yield stress, and total elongation for Sn–5Sb, Sn–5Sb–0.7Ag and Sn–5Sb–0.7Cu solder alloys at 90 °C.

an increase in both UTS and YS with increasing strain rate, indicating that the tensile behavior of the three solder alloys is strain rate dependant. These results are consistent with the previous findings [9,19] that the tensile behavior of the Sn-based alloys often exhibits a strong dependence on the strain rate, or high strain rate sensitivity. The sparse distribution of soft SbSn particles in Sn–5Sb binary alloy seems to cause small strength among the three solder alloys investigated (Fig. 3a). On contrast, the UTS of Sn–5Sb–0.7Cu is greater than those of other two solders over the strain rate range investigated, and is approximately 1.25 times that of Sn–5Sb. Moreover, the YS of Sn–5Sb–0.7Cu is approximately 1.75 times higher than that of Sn–5Sb. However, it is possible to explain the increase in UTS not only by the increase in the volume fraction of IMCs in the ternary alloys, but also with the nature of the atomic bonding forces between the constituents of IMCs. For that reason, the fine needle-like Cu_6Sn_5 IMCs with highest aspect ratios may constrain plastic flow during tensile deformation. On the other hand, the elongation for all alloys was decreased with increasing strain rate. Nevertheless, the Sn–5Sb–0.7Cu alloy exhibits larger elongation than that of the binary Sn–5Sb and Ag-containing alloys at low and high strain rates. Such change in UTS, YS and elongation can be reflected by the microstructural changes observed in Figs. 1, 2 and 3, where the morphology of large equiaxed β-Sn grains β-Sn phase in the Sn–5Sb alloy is gradually changes to a relatively fine β-Sn grains with the addition of Ag and Cu (Fig. 2). Alam et al. [9] had also obtained similar results in Sn–5Sb, Sn–5Sb–3.5Ag and Sn–5Sb–1.5Au lead-free solder alloys.

The both phenomenon of tensile strength and elongation can also be explained by the dislocation multiplication and dislocation interaction, i.e. the IMCs or precipitates formed by Ag and Cu additions were able to generate an additional obstacles for dislocation motion at the grain boundary (the maximum region of mismatch) and inside β-Sn matrix. The dislocation piles up can results in an increase of tensile strength. This means that at high strain rates, the tensile stress increases, since a process of recovery does not takes place. For Cu additions, larger elongation than the binary Sn–5Sb implies that the interaction between IMCs or precipitates with the dislocation motion is strain rate dependent. That means; at low strain rates, the precipitates hinder the fast moving dislocation. With increasing the strain rates, IMCs cannot capture the moving dislocation any more due to a faster velocity of the dislocation in the alloy with increasing the strain rate as reported previously [17,19].

3.5. Effect of temperature on the mechanical properties

The mechanical behaviors at different temperatures were defined a very crucial thermo-mechanical property. This implies that the thermal activated process, such as dynamic recovery, may take place during tensile deformation. It is thought that the recovery process can cause softening in the Sn–5Sb-based alloys through the annihilation of microstructural point and line defects (dislocations, pinning locations, vacancies, etc.) [3]. Fig. 8 illustrates the ability of deformation temperature to decrease the mechanical properties of each solder at constant strain rate. It can be seen that the UTS and YS of the three solder alloys decrease constantly with increasing temperature. Increasing the deformation temperature will initiate rearrangement of the dense dislocation networks formed by strain hardening into simple and more ordered ones. This reduces the lattice energy and therefore lowers the values of UTS and YS at higher temperatures. Moreover, the dislocations have much more energy and can overcome tiny IMCs particles that existed in the β-Sn-matrix. From Fig. 8, the UTS of Sn–5Sb is little smaller than that of Sn–5Sb–0.7Ag alloy while, the UTS of Sn–5Sb–0.7Cu is approximately 18% greater than that of Sn–5Sb, indicating that Ag–Sn and Cu–Sn IMCs particles have a

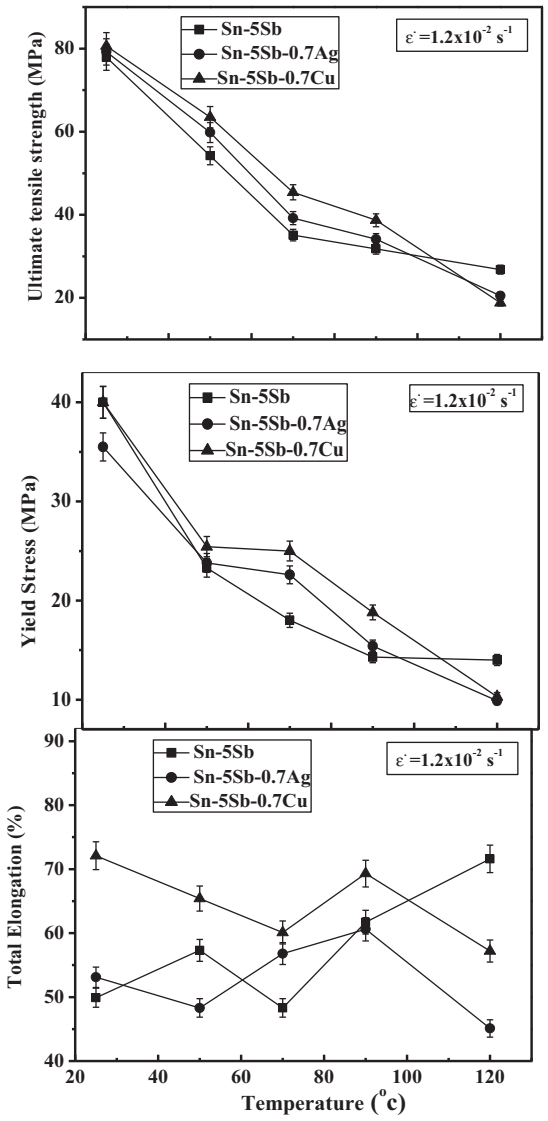

Fig. 8. Effect of temperature on: ultimate tensile strength (UTS), yield stress, and total elongation for Sn–5Sb, Sn–5Sb–0.7Ag and Sn–5Sb–0.7Cu solder alloys at strain rate of $1.2 \times 10^{-2}\ s^{-1}$.

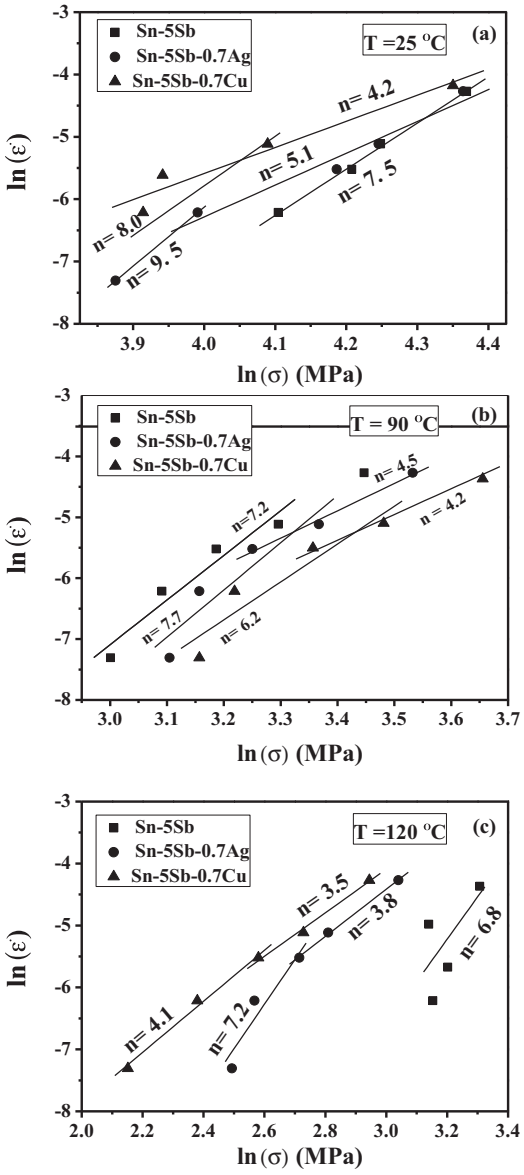

Fig. 9. Applied stress dependence on the steady-state creep strain rate for determination stress exponent (n) values at temperature (a) $T = 25\,^{\circ}C$, (b) $T = 90\,^{\circ}C$ and (c) $T = 120\,^{\circ}C$ for Sn–5Sb, Sn–5Sb–0.7Ag and Sn–5Sb–0.7Cu solder alloys.

notable strengthening effect when the deformation is controlled by dislocation-particle interaction mechanism. Hence, the ternary alloys exhibit a much higher strength than the binary Sn–5Sb alloy at the same strain rate and temperatures. Although this difference in UTS and YS is nearly constant at all the temperature range (except at 120 °C), the ductility as measured by percent elongation has decreased and increased with inconsistent behaviors for all the three solder alloys (Fig. 8). Even though the ductility is limited in the range of 48–72%, the Sn–5Sb–0.7Cu has combination of higher ductility and strength than the other two alloys over the temperature range investigated (except at 120 °C). Several possible explanations exist for sensitivity of ductility to testing temperatures. These include compositional and heat treatment effects on the matrix phase and IMC chemistries, impurity segregation to interfaces, the nature of interface formed between the IMCs and the matrix, the growth rate and stability of the soft and hard IMCs in the alloy matrix, the change of strain rate sensitivity (m) or stress exponent (n) with temperature and the decrease of strain rate with progress in deformation at constant cross-head, instead of constant true strain rate.

3.6. Stress exponents and activation energy

Tensile deformation mechanisms are identified by the values of n and the activation energy Q. In fact, deformation of polycrystalline materials at temperatures above $0.5T_m$ can take place by different deformation mechanisms, associated with different stress exponent values. Dislocation mechanism occurs as a result of viscous glide (stress exponent $n \approx 3$) or dislocation climb (stress exponent $n \geq 4$), but diffusional creep is associated with n values around 1 and grain boundary sliding leads to n values close to 2 (33–35). Since the relationship of stress–strain of Sn-based solder alloys is usually expressed by the power-law of the type [25]:

$$\varepsilon' = A\,\sigma^n \exp\left(\frac{-Q}{RT}\right) \quad (1)$$

where A is a constant and n is the stress exponent. A plot of logarithm of ε' versus the logarithm of σ yields a straight line with slope (n) which determines the mechanism of creep deformation. Fig. 9 compares the three alloys for the steady strain rate versus

Table 5
Activation energy (Q) and stress exponent (n) values at low (σ_{Low}) and high (σ_{High}) stresses for Sn–5Sb, Sn–5Sb–0.7Ag and Sn–5Sb–0.7Cu solder alloys.

Alloy	Temperature (°C)	*n*-values		Q (kJ/mol)
		σ_{Low}	σ_{High}	
Sn–5Sb	25	7.5	7.5	89.0
	90	7.2	7.2	
	120	6.8	6.8	89.0
Sn–5Sb–0.7Ag	25	9.5	5.1	63.3
	90	7.7	4.5	
	120	7.2	3.8	104.0
Sn–5Sb–0.7Cu	25	8.0	4.2	
	90	6.2	4.2	
	120	4.1	3.5	

applied stress curves. The calculated stress exponents at different temperatures are listed in Table 5. In contrast to the binary Sn–5Sb alloy that exhibits a single stress exponent, the ternary alloys with 0.7 Ag or 0.7 Cu show a higher stress exponent at lower stresses and a lower stress exponent at higher stresses. Such transitions in the stress exponent suggest the operation of a threshold stress. Besides, the ternary alloy with 0.7 Cu is the most tensile strength alloy (at stresses below about 57.4.0 MPa). The fine size and needle-like Cu_6Sn_5 shape often may constrain plastic flow during tensile deformation because the height of the climb barrier is large, which hinders dislocation climb and improves tensile deformation behavior. Similar results are observed by Guo et al. [24]. On the other hand, the Sn–5Sb–0.7Cu solder has a crossover point in common with the binary Sn–5Sb alloy near 75 MPa at room temperature, where the tensile strength is similar. Fig. 9(b) and (c) show the 90 and 120 °C tensile data, which illustrate similar trend as observed at room temperature. At 90 °C, it is interesting to note similar strain rates for stresses that are about half of the room-temperature values. It is also evident that the binary Sn–5Sb alloy tensile data obeys the power law relation, but the ternary alloys exhibit high stress exponents at lower stress due to the operation of a temperature-dependent threshold stress, above which a particular deformation mechanism is able to operate. Similar trends are observed in near-eutectic Sn–Ag solders containing small amount of alloy additions [24].

However, Table 5 shows that the n values of the three solder alloys are comparable to the *n* values of 6–8.6 at 27–100 °C for pure tin, 5.5–9.8 at 27–100 °C for Sn–8.1Sb and 5–7.6 at 23–150 °C for Sn–3.5Ag, and Sn–5Sb, which are typical of dislocation climb-controlled creep [3]. Other results obtained in tensile creep tests on cast and homogenized Sn–5Sb, Sn–5Sb–0.7Ag and Sn–5Sb–0.7Cu alloys at high stress levels and low temperature range (from 25 to 70 °C) are characterized by n values in the range of 5.1–10.7, while at low stress levels and high temperature region (120 °C), n was approximately equal to 5–7.5 [6]. Nonetheless, the variations in n can be explained by differences in testing methods, microstructure, specimen preparation, measuring errors, and data processing method.

The activation energy under constant strain rate, *Q*, can be calculated by the following equation deduced from Eq. (1):

$$Q = Rn \frac{\partial \ln \sigma}{\partial \left(1/T\right)} \quad (2)$$

Q values can be estimated from the standard Arrhenius plot of $\ln \sigma$ versus $1000/T$ as shown in Fig. 10. The mean Q values were found to be 89.0, 63.3–104 and 85–90 kJ mol^{-1} for Sn–5Sb, Sn–5Sb–0.7Ag, and Sn–5Sb–0.7Cu solders, respectively, in the temperature range of 25–120 °C. These values were found to be in accordance with that obtained in previous work [3]. The stress exponent and activation energy obtained in this study, compared with the results from the analysis on pure tin [21], suggest also that tensile deformation can

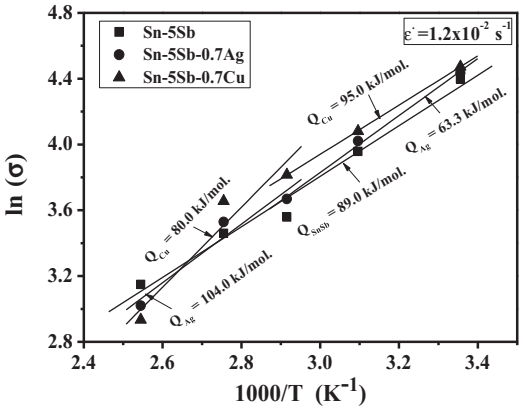

Fig. 10. The activation energy (*Q*), values of the given solder alloys: Sn–5Sb, Sn–5Sb–0.7Ag and Sn–5Sb–0.7Cu.

take place by lattice-diffusion-controlled dislocation climb. Generally, the additions of second-phase particles can affect the distance that dislocations glide between obstacles and the forces that cause them to climb. However, several activated processes can occur in particle-strengthened materials, such as particle by-pass by dislocation climb, Orowan by-pass, and attractive interactions between dislocations and particles. The large values of stress exponent are often observed in dispersion-strengthened alloys due to the attractive interaction between dislocations and particles.

4. Conclusions

Tensile tests for Sn–5Sb, Sn–5Sb–0.7Ag, and Sn–5Sb–0.7Cu solders were conducted. The effects of Ag and Cu addition on the microstructures and mechanical properties of solders were investigated. The effects of strain rate and temperature on the mechanical properties of solders were also studied. Some important results and conclusions are summarized as follows:

From microstructure examination, the SbSn IMC is precipitated within the β-Sn matrix in the pure Sn–5Sb-based lead-free solder alloys. The two ternary alloys Sn–5Sb–0.7Ag and Sn–5Sb–0.7Cu exhibited additional Ag_3Sn, Cu_3Sn and Cu_6Sn_5 IMC phases, respectively. The Ag_3Sn, Cu_3Sn and Cu_6Sn_5 particles contributed to a dispersion strengthening effect to the Sn–5Sb alloy with Ag and Cu additions.

The addition of Ag and Cu decreases the melting point of Sn–5Sb solder alloy from 239. 2 °C to 236.9 and 233.8 °C, respectively.

The Sn–5Sb–0.7Cu alloy had both the highest UTS and elongation, while Sn–5Sb alloy had the lowest one. The formation of fine β-Sn grain size and distribution of fine needle-like Cu–Sn IMC phases in the Sn–5Sb–0.7Cu solder matrix were the main source of the strengthening mechanism.

Sn–5Sb–0.7Ag alloy has the second largest strength at all investigated strain rate and temperature range, which can be attributed to the nature of the atomic bonding forces between the constituents of IMCs and the βSn matrix.

Compared with the two ternary alloys, the sparse distribution of small volume fraction of SbSn IMC particles in Sn–5Sb binary alloy seems to cause the small strength among the three solder alloys investigated.

For all alloys, both UTS and YS increased with increasing strain rate and decreased with increasing temperature, whereas the ductility changes were generally large for the ternary Sn–5Sb–0.7Cu alloy.

The obtained Q and *n*-values were in good agreement with those reported for conventional creep testing of dispersion-strengthened alloys and suggest that tensile deformation can take place by

lattice-diffusion-controlled dislocation climb in Sn–5 Sb-based alloys in the temperature range of investigation.

References

[1] A.K. Gain, T. Fouzder, Y.C. Chan, A. Sharif, N.B. Wong, W.K.C. Yung, J. Alloys Compd. 506 (2010) 216–223.
[2] R.M. Shalaby, J. Alloys Compd. 480 (2009) 334–339.
[3] A.A. El-Daly, Y. Swilem, A.E. Hammad, J. Alloys Compd. 471 (2009) 98–104.
[4] R. Novakovic, D. Giuranno, E. Ricci, S. Delsante, D. Li, G. Borzone, Surface Sci. 605 (2011) 248–255.
[5] Yu. Plevachuk, W. Hoyer, I. Kaban, M. Köhler, R. Novakovic, J. Mater. Sci. 45 (2010) 2051–2056.
[6] A.A. El-Daly, A.Z. Mohamad, A. Fawzy, A.M. El-Taher, Mater. Sci. Eng. A 528 (2011) 1055–1062.
[7] A.K. Gain, T. Fouzder, Y.C. Chan, A. Sharif, W.K.C. Yung, J. Alloys Compd. 489 (2010) 678–684.
[8] A.A. El-Daly, Y. Swilem, M.H. Makled, M.G. El-Shaarawy, A.M. Abdraboh, J. Alloys Compd. 484 (2009) 134–142.
[9] M.E. Alam, S.M.L. Nai, M. Gupta, J. Alloys Compd. 476 (2009) 199–206.
[10] Q.S. Zhu, Z.G. Wang, S.D. Wu, J.K. Shang, Mater. Sci. Eng. A 502 (2009) 153–158.
[11] A.R. Geranmayeh, R. Mahmudi, J. Mater. Sci. 40 (2005) 3361.
[12] R. Mahmudi, A.R. Geranmayeh, A. Rezaee-Bazzaz, Mater. Sci. Eng. A 448 (2007) 287.
[13] S.W. Chen, A.R. Zi, P.Y. Chen, H.J. Wu, Y.K. Chen, C.H. Wang, Mater. Chem. Phys. 111 (2008) 17–19.
[14] A.R. Geranmayeh, R. Mahmudi, J. Electron. Mater. 34 (2005) 1002–1009.
[15] S.W. Chen, C.C. Chen, W. Gierlotka, A.R. Zi, P.Y. Chen, H.J. Wu, J. Electron. Mater. 37 (7) (2008) 992–1002.
[16] Q. Zeng, J. Guo, X. Gu, X. Zhao, X. Liu, J. Mater. Sci. Technol. 26 (2) (2010) 156–162.
[17] C. Wei, Y. Liu, Z. Gao, R. Xu, K. Yang, J. Alloys Compd. 468 (2009) 154–157.
[18] S.K. Das, A. Sharif, Y.C. Chan, N.B. Wong, W.K.C. Yung, J. Alloys Compd. 481 (2009) 167–172.
[19] A.A. El-Daly, A.E. Hammad, Mater. Sci. Eng. A 527 (2010) 5212–5219.
[20] F. Wang, M. O'Keefe, B. Brinkmeyer, J. Alloys Compd. 477 (2009) 267–273.
[21] M.D. Mathew, H. Yang, S. Movva, K.L. Murty, Metallurg. Mater. Trans. A 36 (2005) 99–105.
[22] A.A. El-Daly, A.E. Hammad, J. Alloys Compd. 505 (2010) 793–800.
[23] F.X. Che, W.H. Zhu, S.W. Edith, X.W. Poh, X.R. Zhang, X.W Zhang, J. Alloys Compd. 507 (2010) 215–224.
[24] F. Guo, S. Choi, K.N. Subramanian, T.R. Bieler, J.P. Lucas, A. Achari, M. Paruchuri, Mater. Sci. Eng. A 351 (2003) 190–199.
[25] R. Mahmudi, A.R. Geranmayeh, H. Khanbareh, N. Jahangiri, Mater. Des. 30 (2009) 574–580.
[26] J. Shen, Y.C. Chan, J. Alloys Compd. 477 (2009) 552–559.